



**Model development for enzymatic reactive crystallization of  
 $\beta$ -lactam antibiotics: A reaction-diffusion-crystallization  
approach**

Journal:	<i>Reaction Chemistry &amp; Engineering</i>
Manuscript ID	RE-ART-07-2020-000276.R1
Article Type:	Paper
Date Submitted by the Author:	01-Sep-2020
Complete List of Authors:	Salami, Hossein; Georgia Institute of Technology, School of Chemical and Biomolecular Engineering Lagerman, Colton; Georgia Institute of Technology, School of Chemical and Biomolecular Engineering Harris, Patrick; Georgia Institute of Technology, School of Chemical and Biomolecular Engineering McDonald, Matthew; Georgia Institute of Technology, School of Chemical and Biomolecular Engineering Bommarius, Andreas; Georgia Institute of Technology, School of Chemical and Biomolecular Engineering Rousseau, Ronald; Georgia Institute of Technology, School of Chemical and Biomolecular Engineering Grover, Martha; Georgia Institute of Technology, School of Chemical and Biomolecular Engineering

# Model development for enzymatic reactive crystallization of $\beta$ -lactam antibiotics: A reaction-diffusion-crystallization approach

Hossein Salami<sup>1</sup>, Colton E. Lagerman<sup>1</sup>, Patrick R. Harris<sup>1</sup>, Matthew A. McDonald<sup>1</sup>, Andreas S. Bommarius<sup>1</sup>, Ronald W. Rousseau<sup>1</sup>, Martha A. Grover<sup>1\*</sup>

<sup>1</sup>School of Chemical and Biomolecular Engineering, Georgia Institute of Technology, Atlanta, GA, USA

Enzymatic reactive crystallization of  $\beta$ -lactam antibiotics provides a promising method for efficient and large-scale manufacturing. Since practical processes rely on immobilized enzyme for operation, a robust process model needs to take into account three phenomena of enzymatic reaction, species diffusion, and crystallization of the products. In this work a mathematical model and a numerical simulation procedure are developed for enzymatic reactive crystallization using penicillin G acylase immobilized on a porous carrier. Enzymatic reaction is described using previously established kinetic parameters for a commercial enzyme. An experimentally measured diffusivity is used to model the mass transport resistance, and a 1-D population balance model is used for crystallization of needle-like crystals from supersaturated species. The effect of five immobilization parameters, loading, carrier type and size, enzyme distribution, and carrier size distribution is systematically investigated using the developed model and their implications are discussed for synthesis of two  $\beta$ -lactam antibiotics, ampicillin and cephalixin, with different turn over rates. As expected, using carriers with larger radius, higher loading, and smaller diffusivity are shown to lead to significant mass transport resistance and deviation from free enzyme behavior. This effect is more drastic for the ampicillin system, which has a faster dynamics due to lower affinity of enzyme for its nucleophile agent. Testing different enzyme distributions, it is shown that accumulation of enzyme at the outer regions of the carrier leads to an improved process and mitigation of mass transport resistance due to higher sensitivity of diffusion timescale to radius, compared to reaction timescale to enzyme concentration. Adding a crystallization module to the model allowed for dynamic modeling of processes with high substrate concentrations applicable to reactive crystallization. Effect of pH as a critical process parameter affecting both reaction and crystallization is discussed, as well as potential intra-carrier crystallization and consequent enzyme blockage.

## 1 Introduction

$\beta$ -lactam antibiotics such as ampicillin and cephalixin are among the most widely used antibiotic Active Pharmaceutical Ingredients (APIs) [1, 2]. Classical chemical routes for

production of these APIs face challenges such as requiring low operating temperatures and using organic solvents [3]. On the other hand, enzymatic synthesis offers a green alternative and is currently the prevalent method of manufacturing [2]. The enzyme penicillin G acylase (PGA) can catalyze the reaction between an activated acyl donor (*e.g.*, phenylglycine methyl ester, PGME) and a nucleophilic molecule containing the  $\beta$ -lactam core (*e.g.*, 7-aminodesacetoxy-cephalosporanic acid (7-ADCA) or 6-aminopenicillanic acid (6-APA)) to produce the antibiotic (*e.g.*, cephalexin or ampicillin) [4]. Figure 1 illustrates the main reactions involved in this system. Besides API synthesis, two additional side reactions occur in which PGA catalyzes the hydrolysis of the activated acyl donor or the API itself to produce an undesired byproduct (phenylglycine, PG). Allowing the system to proceed to its thermodynamic equilibrium state would result in low process yields as the target antibiotic is an intermediate in the overall reaction network. To avoid this issue and achieve acceptable process attributes, the process time and operating conditions need to be optimized; *i.e.*, the process needs to be kinetically controlled [5]. A comprehensive review on challenges associated with enzymatic synthesis of  $\beta$ -lactam antibiotics is presented by Giordano *et al.* [3]. Besides engineering the enzyme to increase its selectivity towards API synthesis (routinely referred to as synthesis-to-hydrolysis (SH) ratio [4, 6]), another method for improving this process is protecting the antibiotic molecule from hydrolysis by isolating it through crystallization. To induce crystallization, the product must be generated in large enough quantities to exceed its thermodynamic solubility and generate supersaturation, the driving force for crystallization. Combining the reaction and crystallization steps into one, is referred to as a reactive crystallization process. Reactive crystallization provides a method for *in-situ* product removal, can improve the process yield, and potentially simplify downstream processing [7, 8, 9].

There are many reports in the literature focusing on different aspects of this reactive crystallization process. Mostly of experimental nature, these typically deal with only one of the enzymatic reaction or crystallization steps. PGA (soluble or immobilized) activity in

catalyzing the reaction network of Figure 1 has been studied by several groups under different experimental conditions and using different enzyme variants. Furthermore, physically-based, or black-box models such as artificial neural networks have been developed and tuned to match the experimental data [4, 5, 6, 7, 10, 11, 12]. These studies are typically performed at low concentrations to avoid crystallization that would not be easy to decouple from the reaction rate. On the other hand, several studies focused on understanding the crystallization of  $\beta$ -lactam antibiotics and gathering the relevant data. For example, solubility as a key parameter in crystallization has been measured for ampicillin, amoxicillin and cephalexin under a variety of conditions [13, 14, 15, 16]. Some of these studies also used carefully designed and controlled experiments utilizing Process Analytical Technologies (PAT) [17] to observe the system and gather the information related to crystallization kinetics. Taking the similar approach as the reaction-focused studies, these studies typically avoid complicating the system's dynamics by not introducing the reaction. Instead, externally controlled pH is typically used to induce crystallization, simulating a reaction with short timescale and simplifying the system response. Building on these works, some studies aimed at optimizing these systems under certain conditions. For example, Fan *et al.* [18] performed extensive experiments to experimentally optimize the feed profile of the substrate in a fed-batch system for production of cephalexin using a commercial PGA. In a series of articles Gerogiorgis *et al.* [19, 20] used the available information on the reaction and crystallization kinetics to perform dynamic modeling and optimization of batch systems for production of dissolved amoxicillin, and ampicillin crystals. McDonald *et al.* [21] proposed a continuous process for production of  $\beta$ -lactam antibiotics crystals via the enzymatic route and constructed a Pareto-optimal surface for process productivity, yield and conversion.

One of the important challenges in enzymatic synthesis is the recovery of the enzyme for multiple uses. This is especially important for realization of continuous manufacturing processes for production of  $\beta$ -lactam antibiotics. Products in this process are of less value compared to the enzyme so enzyme recovery is important to ensure economic viability.

To facilitate the enzyme/product separation and for recovering the enzyme, it needs to be immobilized on a support. A variety of organic and inorganic supports are available for immobilizing the PGA by different surface chemistries such as covalent bonding, adsorption, or ion-exchange. An ideal support should be mechanically stable, and show no enzyme leakage during the process. Furthermore it should provide sufficient surface area and immobilization sites for loading the required amount of enzyme. The last criteria can limit the maximum acceptable size range for a non-porous support where only the outer surface is available for enzyme immobilization. On the other hand, different polymeric porous beads provide plenty of available surface and can accept a large range of enzyme loadings. Moreover, the enzyme immobilized inside a porous structure is better protected against the shear stress [22]. A detailed review on different immobilization strategies for PGA can be found elsewhere [23]. The drawback of using porous beads is that depending on the reaction timescale and structure of the carrier, enzyme may show a significantly different apparent activity and selectivity compared to the free enzyme, due to mass transfer limitations.

In an enzymatic reactive crystallization process, the three phenomena of enzyme-catalyzed reaction, species transport to and from the active site of biocatalyst, and crystallization of the API (and potentially other species) exhibit a complex interplay that determines the overall process dynamics. Timescales associated with each step can widely vary based on factors such as pH-dependent enzyme activity, carrier size and structure, and API solubility, deciding the rate determining step and ultimately the final process attributes under different conditions. A robust process model applicable to a wide range of conditions needs to take into account all of the mentioned phenomena. Such model forms the backbone for model-based decision making, and process design, optimization, and control. In this work, we use previously established kinetic data for enzymatic synthesis of ampicillin and cephalexin using free PGA and reported crystallization parameters for both systems to develop a process model for the enzymatic reactive crystallization of  $\beta$ -lactam antibiotics using PGA immobilized on a porous carrier. Beginning with studying each phenomenon



carriers were considered in this study: Highly porous glyoxyl-agarose carrier, previously characterized by Valencia *et al.* [24], and two types of commercially available methacrylic-based polymeric beads, Immobead (COV2) and ReliZyme<sup>TM</sup> (S grade). All have covalent attachment sites. Immobeads were obtained from ChiralVision, Netherlands and ReliZyme carriers were kindly donated by Resindion, Italy for estimation of diffusion parameters. Effective diffusion coefficient,  $D_e$ , for cephalixin molecules in both carriers was measured using effusion experiments [24, 25], details of which are presented in the Supporting Information. For other species,  $D_e$  was estimated based on the value found for cephalixin and their molecular weights using Vorlop’s equation [25]. Size distributions for both Immobead (COV2) and ReliZyme (S) were determined using optical microscopy followed by image analysis in MATLAB (details presented in the Supporting Information). Crystallization kinetic parameters and solubility values for both APIs are reported in the literature [13, 15, 16] and were used for this study (Table S2 in the Supporting Information).

## 2.2 Model Development

**Reaction.** To model the kinetics of the enzymatic reaction, we adopt the reaction network (RN) introduced by Youshko and Svedas [8], shown in Figure 1(b). Unlike simpler cases, this RN is able to reproduce system behavior at high concentrations of the nucleophile substrate, taking into account its inhibitory effect on API hydrolysis [7, 8, 26]. Previously, McDonald *et al.* [7] showed that addition of two side protonation/deprotonation equilibrium reactions on the acyl-enzyme complex and a pH-dependent nucleophile dissociation constant  $K_n$  are sufficient to describe the change of enzyme activity with pH [7]. For production rate

of the API and the hydrolysis byproduct (PG) we have [8, 21]

$$\frac{dc_p}{dt} = \frac{e}{(k_3K_n + k_4c_n + k_5c_n)} \cdot \left[ \frac{k_2k_4c_n c_s}{K_s} - \frac{k_{-4}c_p(k_3K_n + k_5c_n)}{K_p} \right] \quad (1a)$$

$$\frac{dc_b}{dt} = \frac{e(k_3K_n + k_5c_n)}{(k_3K_n + k_4c_n + k_5c_n)} \cdot \left[ \left( \frac{k_2c_s}{K_s} + \frac{k_{-4}c_p}{K_p} \right) \right] \quad (1b)$$

$$e = \frac{e_0}{\left( 1 + \frac{c_s}{K_s} + \frac{c_p}{K_p} + \frac{c_n}{K_n} + \frac{K_n}{(k_3K_n + k_4c_n + k_5c_n)} \left( \frac{k_2c_s}{K_s} + \frac{k_{-4}c_p}{K_p} \right) \right) \left( 1 + \frac{c_n}{K_n} + \frac{10^{-pH}}{K_{A1}} + \frac{K_{A2}}{10^{-pH}} \right)} \quad (1c)$$

where  $c_s$ ,  $c_n$ ,  $c_p$ , and  $c_b$  are concentrations of acyl donor substrate, nucleophile substrate, API product, and the hydrolysis byproduct;  $e_0$  is the enzyme concentration dictated by the enzyme loading to the biocatalyst during the immobilization, and  $e$  is the available enzyme concentration. Note that for a fixed overall enzyme loading, different locations inside the carrier may have different local enzyme concentrations,  $e_0(r)$ . Parameters used for ampicillin and cephalixin synthesis are presented in Table S1 of the Supporting Information. A key assumption here is that the immobilized enzyme reaction has the same intrinsic kinetic parameters as the free enzyme. This assumption is shown to be robust for PGA immobilized via covalent attachment [11, 24], and is generally valid as long as the enzyme does not undergo strong conformational changes during the immobilization and there is no significant steric or electrostatic effects on the enzyme in its microenvironment [27]. In any case, free enzyme is the most readily available approximation for the behavior of an immobilized enzyme, unless detailed experiments (such as crushing the biocatalyst to minimize the diffusion effect [28]) or computational chemistry studies are performed to investigate the effect of immobilization procedure on intrinsic enzyme activity. If such effects are observed during enzyme immobilization, they can be accounted for in the model by, for example, addition of a new adjustable parameter. Rates of acyl donor and nucleophile consumption can be calculated using Eqn. (1) and conservation of the  $\beta$ -lactam ring and acyl donor moiety.

It is also worth highlighting that all species in this system are either a base (PGME) or an amphoteric compound and may exist in either a charged or neutral state depending on the local pH. It has been suggested that only one state (*e.g.*,  $\text{CEX}^{(-)}$ ) might be the reactive

species for the reaction [11, 29]. In Eqn. (1) we do not distinguish between the different states of each species, and the overall effect of pH on reaction kinetics (either through changing the reactive state or changing the enzyme itself) is captured by  $K_{A1}$ ,  $K_{A2}$ , and  $K_N(pH)$ .

**Diffusion.** Two methods can be used to describe transport of species into and out of the biocatalyst. The more rigorous option is to use a pore-scale approach. However, detailed structural information about the carrier and large computational resources for discretizing the domain are necessary [30, 31]. Alternatively, one can take a continuum approach by considering the biocatalyst as a homogeneous medium with an effective diffusivity for each species. The second approach has been shown to provide good predictions for enzymatic and other catalytic systems without demanding heavy computations [24, 29, 32, 33]. Considering a spherical bead and assuming fast diffusion through the biocatalyst boundary layer due to good mixing in the reactor (*i.e.*, no external mass transport resistance), the conservation equation for each species  $i$  in radial coordinates becomes

$$\frac{-1}{r^2} \frac{d}{dr} (r^2 \cdot J_i) - R_i(c, e_0, pH) = \frac{dc_i}{dt} \quad (2)$$

where the reaction term  $R_i(c, e_0, pH)$  is described by Eqn. (1) and is a function of local concentrations and pH. Considering that some of the involved species are amphoteric compounds and might be present partially in a charged state, and that ions such as  $\text{Na}^+$  and  $\text{Cl}^-$  are used as titrant, the Nernst-Planck equation can be used to calculate the flux of each species in Eqn. (2), according to [29]:

$$J_i = -D_{e,i} \left[ \frac{dc_i}{dr} - z_i c_i \frac{\sum_{n=1}^N z_n D_{e,n} \frac{dc_n}{dr}}{\sum_{n=1}^N z_n^2 D_{e,n} c_n} \right] \quad (3)$$

where  $z_i$  is the charge of each species. According to Eqn. (3), the flux of each species in the system is the sum of (1) flux in its concentration gradient (Fick's law), and (2) flux in its

charged state which is calculated based on its concentration gradient and the concentration of other charged species.  $D_{e,i}$  is the effective diffusivity for each species, which depends on factors such as molecule size, cosolute concentrations, carrier structure, hydrophobicity, surface charge, etc. [32, 34, 35]. Typically,  $D_{e,i}$  is estimated using the experimental method of Grunwald [25]. Here, we study two types of carriers with different structural properties and diffusivities: (1) highly porous glyoxyl-agarose carriers and (2) commercial methacrylic-based carriers Immobead (COV2) and ReliZyme. Experimental values for  $D_e$  of relevant components are reported for glyoxyl-agarose carriers by Valencia *et al.* [24]. Figure 2 shows the result of the effusion experiments for cephalexin molecules in Immobeads and ReliZyme carriers. Following Grunwald [25], the effective diffusivity can be estimated by fitting the data with the equation

$$c(t) = c_\infty \left[ 1 - e^{\left(\frac{-\pi^2 D_e}{R^2}\right)t} \right] \quad (4)$$

where  $c_\infty$  is the concentration at extended times and  $R$  is the mean radius of carrier particles.  $D_e$  for other species were estimated by Vorlop’s equation ( $D_e \propto M_w^{-0.41}$ ) using cephalexin diffusivity as a reference. Effective diffusivity values have also been reported for another type of commercial carrier, Assemblase<sup>®</sup>, by van Roon *et al.* [29]. Table 1 lists the values used for the effective diffusion coefficient for each species for the three carriers mentioned.

Table 1. Effective diffusivities  $D_{e,i}$  ( $\frac{m^2}{s} \times 10^{10}$ ) for three types of porous carriers under study. <sup>a</sup> Values for Agarose beads are from Ref. [24], and  $D_{e,Na^+}$  and  $D_{e,Cl^-}$  from Ref. [29]. Values for ReliZyme (S) and Immobead (COV2) carriers were measured in this study and were very similar.  $D_{e,CEX}$  is approximated by fitting the effusion data with Eqn. (4) using a least squares regression. Mean radius used for Immobeads was 190  $\mu\text{m}$ , and 85  $\mu\text{m}$  for ReliZyme beads.

Carrier	$D_{e,PGME}$	$D_{e,7-ADCA}$	$D_{e,CEX}$	$D_{e,PG}$	$D_{e,Na^+}$	$D_{e,Cl^-}$
Immobead (COV2)	2.44	2.19	1.8	2.53	10	15
ReliZyme (S)	2.3	2.1	1.7	2.39	10	15
Agarose <sup>a</sup>	5.65	5.71	5.09	5.68	10	15

As a final note on Eqn. (2), it is worth mentioning that since reaction parameters were measured based on the overall concentration of each species (not distinguishing between

neutral and charged states), here we take the vector of overall concentrations as the system concentration state. However, when calculating  $J_i$ , the amount of each form, charged or neutral, is calculated using the Henderson–Hasselbalch equation based on the local pH and the corresponding  $pK_a$  values for each species. The local pH at different locations inside the biocatalyst environment can be calculated assuming electroneutrality and using the local concentration of each species, its  $pK_a$ , and the water dissociation constant,  $K_w$  [21, 36, 37].  $pK_a$  values used for each species are presented in the Supporting Information.

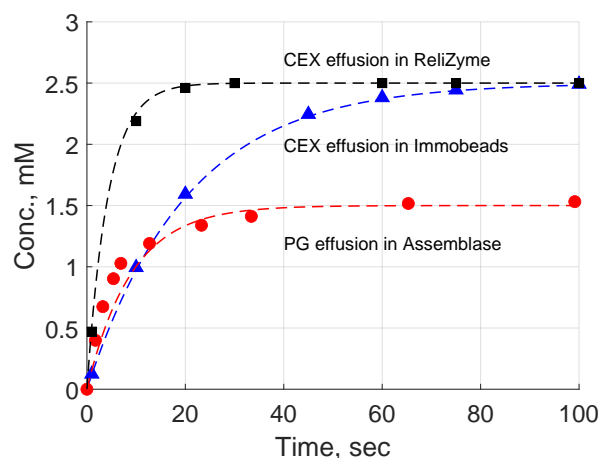


Fig. 2. Effusion data for measuring the effective diffusivity of cephalixin in Immobead (COV2) and ReliZyme (S) carriers. Data were used with Eqn. (4) to estimate the effective diffusivity,  $D_{e,CEX}$ . Mean radius used for Immobeads was  $190 \mu\text{m}$ , and  $85 \mu\text{m}$  for ReliZyme beads. Data for PG diffusivity in Assemblase<sup>®</sup> carrier [29] are shown for comparison.

Equation (2) can be solved using a set of initial concentrations and boundary conditions at the center of the carrier and its interface with the bulk fluid.

$$\left. \frac{dc_i}{dr} \right|_{r=0} = 0 \quad (5a)$$

$$J_i \cdot \frac{A_{cat}}{V_b} \bigg|_{r=R} = \frac{dc_{i,bulk}}{dt} \quad (5b)$$

where  $A_{cat}$  is the total catalyst outer surface area,  $V_b$  is the volume of the bulk phase, and  $c_{i,bulk}$  is the bulk concentration for each species.

**Crystallization.** Typically, relatively high acyl-donor and nucleophile concentrations

are used in enzymatic synthesis to improve the nucleophile conversion and the SH ratio [4, 7]. This, in combination with the limited solubility of both API and the hydrolysis byproduct [16, 14], may result in a solution supersaturated with respect to one or both species at some point during the synthesis process. Supersaturation is defined as  $S = c/c^*$ , where  $c$  is solute concentration and  $c^*$  its solubility; it is the driving force behind crystallization and determines the rate of both nucleation (*i.e.*, formation of stable nuclei that can grow to become crystals) and growth. In general, solubility  $c^*$  is a function of pH, temperature, ionic strength, and concentration of cosolutes. Solubilities of both ampicillin and cephalexin in water at 25 °C and over a range of pHs are reported by Santana *et al.* [14] and McDonald *et al.* [16] and are shown in Figure S1 in the Supporting Information. The effect of solution ionic strength on solubility can be realized by adjusting the  $pK_a$  values to take into account the solution nonideality. Using the extended Debye-Huckel theory for activity coefficient [38], and  $I$  as the ionic strength we have

$$pK_{a,j} = pK_{a,j}^0 + 0.509 \times (2z_j - 1) \left( \frac{\sqrt{I}}{1 + \sqrt{I}} - 0.2I \right) \quad (6)$$

Note that the byproduct PG also is sparingly soluble in water ( $c_{PG}^* \sim 35 - 39$  mM at 25 °C and pH 5.5 – 7.5 [14]) and might crystallize if generated at higher concentrations. This is, of course, undesired and results in an impure solid phase, necessitating additional purification steps. Here, we only model crystallization of the product.

To model the dynamics of the crystallization process, nucleation and growth kinetics need to be considered. Nuclei generation is typically considered to be either by primary nucleation ( $B_1$ ), that is generation of stable nuclei from a clear supersaturated solution, or by secondary nucleation ( $B_2$ ), which depends on existing crystals in the system. Primary

and secondary nucleation rates can be modeled by [16, 15]

$$B_1 = k_{B1} S \exp\left(\frac{-B_0}{\ln^2 S}\right) \quad (7a)$$

$$B_2 = k_{B2} G^b M^m \quad (7b)$$

where  $S$  is the supersaturation,  $M$  is the slurry density (mass of crystals per volume of the solution), and  $G$  is the crystal growth rate

$$G = k_g(S - 1)^g \quad (8)$$

With Eqn. (7) and (8), one can use a population balance to model the birth and growth of crystals over time [15, 16]. For a system with constant volume, and no crystal growth rate dispersion, agglomeration and breakage, the population balance becomes

$$\frac{\partial n(L, t)}{\partial t} + \frac{\partial(n(L, t)G(t))}{\partial L} = 0 \quad (9)$$

with  $n$  as the crystals population density function, and subject to the boundary condition  $n(0, t) = (B_1 + B_2)/G$ . Note that Eqn. (9) assumes that crystal size can be characterized by a single dimension,  $L$ . This is consistent with previous observations of needle-like ampicillin and cephalexin crystals [13, 15, 16, 39].

Crystallization kinetic parameters  $k_{B1}$ ,  $k_{B2}$ ,  $B_0$ ,  $b$ ,  $m$ ,  $k_g$ , and  $g$  in Eqn. (7) and (8) are typically evaluated by fitting the population balance model to experimental data; values for both ampicillin trihydrate and cephalexin monohydrate crystals are reported in the literature [13, 15, 16] and are presented in the Supporting Information. Here, we use the method of moments for solving the population balance model in Eqn. (9). Another alternative is to use the method of lines for solving the system of equations resulting from Eqn. (9) [16]. Unlike the method of moments that uses moments of the crystal size distribution (CSD), the method of lines directly tracks the CSD in time, but with a larger computational cost.

Defining moments of the CSD,  $\mu_i$ , we have:

$$\frac{d\mu_0}{dt} = B_1 + B_2 \quad (10a)$$

$$\frac{d\mu_i}{dt} = i\mu_{i-1}G \quad i = 1, 2, \dots \quad (10b)$$

For a system with no initial crystals, Eqn. (10) has the initial condition of zero for all moments. Nonzero initial conditions should be considered for an initially seeded system. In that case  $\mu_{0,t=0}$  would be the total number of seed crystals per volume of solution,  $\mu_{1,t=0}$  the total length of seed crystals, etc. Slurry density in Eqn. (7) can be calculated using the third moment of the CSD and crystal particle shape factor,  $k_v$  (estimated to be 0.03 for needle-like crystals typical to ampicillin and cephalexin [40]):

$$M = k_v \mu_3 \rho_c \quad (11)$$

Considering the crystallization, Eqn. (5) needs to be augmented and the conservation equation for species in bulk becomes

$$\frac{dc_{i,bulk}}{dt} = J_i \cdot \frac{A_{cat}}{V_b} \Big|_{r=R} - 3k_v \rho_i G_i \mu_{2,i} / M_{w,i} \quad (12)$$

Here we assume that crystallization is limited to species in the bulk phase. Further discussion of this assumption will be presented in Section 3.4. Also, in general, other species in this system such as the byproduct PG may crystallize provided their supersaturation is above unity. If needed, a similar approach can be used to include the crystallization of PG in the model as well.

**Numerical simulation** A typical approach for studying the dynamics of reactive systems subject to diffusion limitations is to use the concepts of effectiveness factor and Thiele modulus to determine whether diffusion of species significantly impacts the apparent kinetics [32]. Relevant expressions for heterogeneous catalysts effectiveness factors have been

established for simple rate laws, including Michaelis-Menten for first order single substrate enzymatic systems [27]. However, as the RN and the corresponding rate equations become more complicated, applicability of general relations becomes limited [41]. For the RN of Figure 1, a two-substrate enzymatic reaction with the intermediate as the target product, formulating analytical expressions for effectiveness factor and Thiele modules becomes challenging. In such cases it is simpler to numerically solve the set of equations formulated above to study the dynamics of the system under different conditions [41, 42].

Having the governing equations for each part of the model, we can now define a system state vector  $\vec{u} = [c_{cat}^{\vec{c}}, c_{bulk}^{\vec{c}}, \vec{\mu}]^T$  containing species concentrations in the discretized biocatalyst domain ( $N \times N_s$  elements where  $N$  is the number of discretization nodes and  $N_s$  number of species), species concentrations in the bulk phase ( $N_s$  elements) and five moments for the product CSD. Depending on the presence of carriers with different representative radii, or crystallization of multiple species, additional elements may be added to the state vector. The biocatalyst spatial domain was discretized using a three-point central finite difference scheme for middle points and a three-point backward scheme for the interface nodes. The discretization transforms Eqn. (2) into a set of ordinary differential equations (ODEs) that then can be integrated in time along with Eqn. (10) and (12) to predict the system's dynamics under different conditions. Integration was performed using the MATLAB software *ode15s* solver appropriate for explicitly solving stiff ODEs. Note that working with a diffusion system, the ratio  $\frac{D_e \Delta t}{\Delta x^2}$  determines the stability of the numerical calculations. Discretizing the spatial domain with a very fine mesh results in a small allowable  $\Delta t$  and prolonged integration times. For this system  $N = 30 - 40$  nodes were used and were sufficient as using a finer mesh did not noticeably alter the simulation results. Also, controlling pH of the bulk phase can be included in the model by calculating the necessary base/acid addition to keep the pH at its fixed value at each timestep during the simulation. Figure S3 in the Supporting Information illustrates the overall framework used for the numerical simulation.

## 3 Results and Discussion

### 3.1 Timescale analysis

Before attempting to solve the system of equations obtained from (1), (2), and (10), helpful insight to the general behavior of the system can be obtained by performing simple timescale analysis. The timescale of the enzymatic reaction is determined by pH, as well as enzyme and reactant concentrations. Note the local immobilized enzyme concentration is a function of enzyme loading into the carrier and may take different values for a fixed total enzyme concentration in the reaction vessel [24]. Different enzyme loadings can be achieved by, for example, changing the protein concentration in the immobilization solution. Note that one might desire to use the highest possible enzyme loading, and therefore minimize the total carrier particle mass and density in the reactor. However, the direct impact of loading on the local enzyme concentration in the carrier can have a significant influence on the interplay between reaction and diffusion rates which in turn determines the biocatalyst effectiveness factor [27]. Here, we perform the timescale analysis on three representative enzyme loadings: 5, 25, and 50  $\frac{\text{mg enzyme}}{\text{g wet carrier}}$  corresponding to  $\sim 65$ , 320, and 635  $\mu\text{M}$  enzyme concentration for a bead density of 1.1  $\frac{\text{g}}{\text{ml}}$ . Taking the continuum-medium approach, we consider the porous carrier as one single unit with a fixed volume. The three loading levels will be referred to as “low”, “moderate”, and “high” loading throughout this manuscript. Clearly, very low enzyme loadings are not practical since the amount of biocatalyst needed to supply a necessary total enzyme concentration in the reactor becomes impractically large. Figure 3 shows the ratio of the necessary biocatalyst volume to the reactor volume as a function of enzyme loading into the biocatalyst for a fixed total enzyme concentration of 5  $\mu\text{M}$ .

To simplify the analysis, we focus on the initial phase of reaction when product concentration is low, and the terms on the right-hand side of Eqn. (1) corresponding to product hydrolysis may be neglected. Considering the complex rate equation in Eqn. (1), different

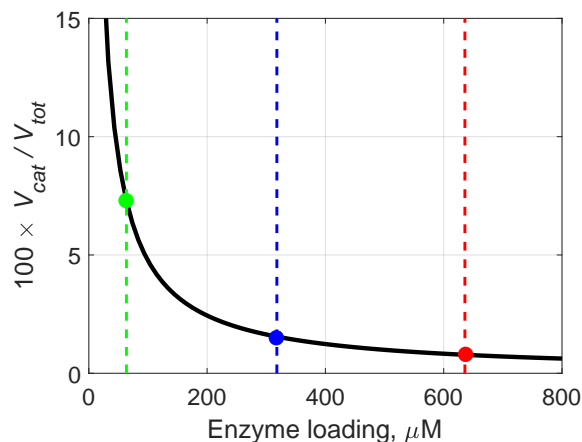


Fig. 3. Ratio of total biocatalyst volume to the total reactor volume at different enzyme loadings into the support for achieving a fixed total enzyme concentration of  $5 \mu\text{M}$  in the vessel. Lower enzyme loadings lead to larger amount of carrier beads necessary to supply a fixed total enzyme concentration in the reactor. Three representative loadings were chosen for further analysis, from left to right: “low”, “moderate”, and “high”.

methods can be used to approximate the reaction timescale. Here, the reaction timescale is calculated as the time required to reach 100% conversion of the acyl donor substrate based on the initial rates in a reaction solution with 0.1 M initial concentration of reactants. The diffusion timescale can be estimated by  $\tau_{diff} \approx R^2/D_e$  and is calculated for two types of carriers with different effective diffusivities (Immobeard-like and Agarose-like). Figure 4 shows the reaction timescale for cephalixin and ampicillin synthesis systems at two different pH values. The two example pH values of 6.3 and 7 were chosen because the enzyme has an acceptable activity and both APIs have limited solubility in this range, making it suitable for a reactive crystallization process. Moreover, both enzyme activity and solubility undergo significant changes with pH in this range. As it can be seen in Figure 4, the reaction timescale decreases by loading higher enzyme concentrations into the biocatalyst which is expected from Eqn. (1). Also, both reactive systems show longer timescale at  $\text{pH} = 6.3$  compared to  $\text{pH} = 7$  as enzyme activity decreases with decreasing pH [7]. Not surprisingly, as the radius of the carrier increases, the timescale of diffusion increases relative to that of the reaction, shifting the rate-determining step towards the former. Comparing the two APIs in different

enzyme loadings and pH values, the cephalaxin system shows a relatively longer reaction timescale, meaning that its synthesis is expected to show less sensitivity to immobilization of the enzyme and the resulting mass transfer limitations [10]. This is investigated in detail in the following section by comparing the dynamics of both systems.

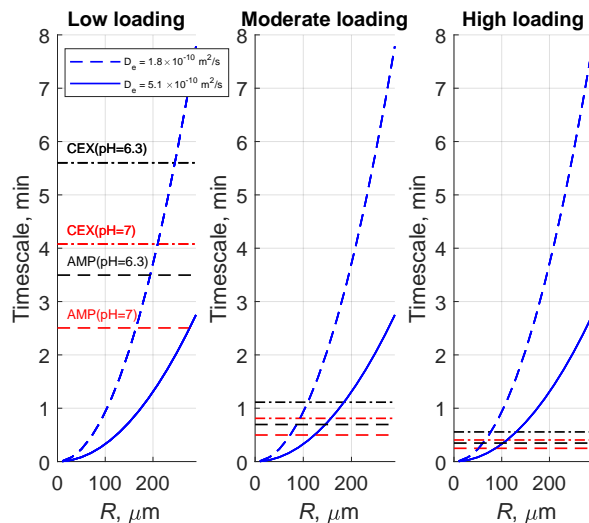


Fig. 4. Timescale analysis for enzymatic synthesis of  $\beta$ -lactam antibiotics, cephalaxin and ampicillin. Horizontal lines show reaction timescale for a reaction with 0.1 M initial concentration of both reactants at different pHs and enzyme loadings into the biocatalyst; -.- corresponds to cephalaxin and -- to ampicillin synthesis. Curves correspond to diffusion timescale in two types of carriers with different structures and effective diffusivities, agarose-like (solid curve,  $D_{e,CEX} = 5.1 \times 10^{-10} \frac{m^2}{s}$ ) and Immobead-like (dashed curve,  $D_{e,CEX} = 1.8 \times 10^{-10} \frac{m^2}{s}$ ) from Table 1.

The above analysis is only meant to provide a general insight to the system and a qualitative comparison between the two APIs and their behavior in a process with immobilized enzyme. Ultimately, reaction and diffusion processes occur simultaneously and unless there is a large difference of several orders of magnitudes between their rates (based on Figure 4, this is only the case for very small carriers with  $R < 20 \mu m$ ), the observed dynamic is affected by both phenomena and can be precisely determined only after numerically solving the system of Equations (1) – (10). Furthermore, the estimation of reaction timescale is based on the assumption of a constant pH. However, in an actual process, even when the bulk pH is fixed, possible concentration and so pH gradients internal to biocatalyst may exist. This

means the enzyme is subjected to a different pH condition than the bulk, which can affect the reaction kinetics. Such complications cannot be addressed by the simple analysis presented above. Finally, we excluded crystallization in this simple analysis since it can occur with a wide range of timescales depending on initial seeding and properties of seed crystals. This is captured by the second moment of the seeds CSD:

$$\tau_{cry} \approx c^*/(3k_v \cdot \mu_2 \cdot k_g \cdot \rho_{cry} \cdot M_w^{-1}) \quad (13)$$

### 3.2 Primary immobilization variables

In order to take advantage of the formulated model for optimizing biocatalyst design with a systematic procedure, one may define three primary variables in biocatalyst preparation: (1) enzyme loading into the carrier, (2) carrier type and structure, and (3) carrier size. These variables can be directly controlled during immobilization experiments. The level of enzyme loading can be adjusted by altering the concentration of protein offered to the carrier in immobilization solution. Carriers with different structures (pore size, tortuosity, etc.) [32] and size can be prepared/purchased depending on specific process needs. Here, we investigate the interplay among these variables by directly solving the set of ODEs describing the system dynamics and compare the two API systems. This also serves to confirm the validity of the timescale analysis. To formalize the procedure, we use three process attributes that typically characterize the performance of  $\beta$ -lactam antibiotics production processes in batch reactors: selectivity, nucleophile conversion, and productivity (all defined at maximum nucleophile conversion).

$$\text{Selectivity} = \frac{c_p}{c_b} \Big|_{t_{max}} \quad (14a)$$

$$\text{Conversion} = 100 \times \left(1 - \frac{c_n}{c_{n0}}\right) \Big|_{t_{max}} \quad (14b)$$

$$\text{Productivity} = \frac{c_p}{t} \Big|_{t_{max}} \quad (14c)$$

where  $t_{max}$  is the point corresponding to maximum nucleophile conversion. Figure 5 shows a typical concentration profile simulated for a batch enzymatic synthesis of cephalixin using 0.1 M initial concentration of both reactants, highlighting the  $t_{max}$  point.

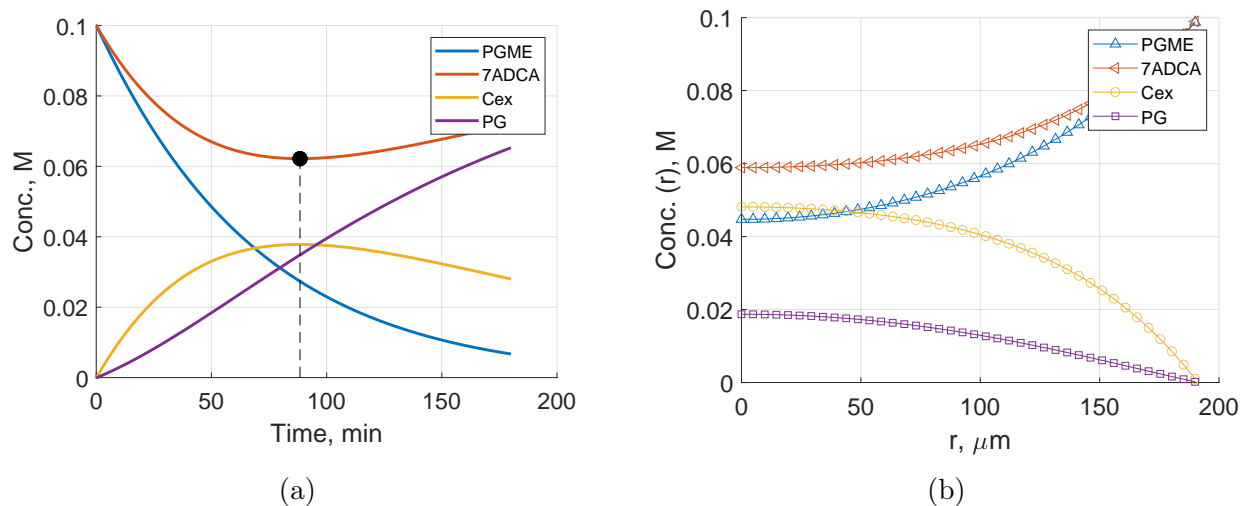


Fig. 5. (a) Simulated time course for cephalixin synthesis using 0.1 M initial concentration of PGME and 7-ADCA, 5  $\mu$ M of PGA immobilized on 190  $\mu$ m Immobead (COV2), at pH = 7. Dashed line shows  $t_{max}$  point. At  $t_{max}$ , from top to bottom curves correspond to 7-ADCA, CEX, PG, and PGME profiles. (b) Example of species distribution inside the carrier at  $t = 1$  min.

Figure 6 shows the effect of carrier size, type, and enzyme loading on the three process attributes defined by Eqn. (14) for cephalixin synthesis. Each attribute is normalized with respect to the free enzyme at the same total enzyme concentration of 5  $\mu$ M and initial concentration of 0.1 M for both substrates. In agreement with preliminary timescale analysis, using carriers with a large radius leads to strong diffusion limitations and significant deviation of all attributes from that of the free enzyme. As the support size decreases, diffusion limitations diminish and reaction becomes the rate-determining step and all process attributes converge to that of the free enzyme. The critical radius below which mass transport limitations practically vanish depends on the level of enzyme loading. Again, this was expected since at higher loadings (*i.e.*, higher local enzyme concentration in the bead) the reaction rate is faster and so the overall dynamics are more sensitive to diffusion rate ( $D_e$  and  $R$ ). The same explanation is applicable to the difference between pH 6.3 and 7. As

it was shown in Figure 4, for both APIs, the reaction timescale is larger (reaction rate is slower) at pH 6.3; therefore, the process is less sensitive to mass transport at this pH. Figures such as Figure 6 can be consulted to decide whether for a specific choice of immobilization carrier and enzyme loading, diffusion limitations significantly impact the dynamics or if it can be approximated using only free enzyme kinetics. For example, examining Figure 6, it is clear that for agarose-like carriers which have a large effective diffusivity, the difference from free enzyme behavior at a radius smaller than  $100\ \mu\text{m}$  is less than 10% for all attributes. This behavior is consistent with experimental results reported by Valencia *et al.* [24] where cephalaxin synthesis experiments using immobilized PGA on agarose beads with radius of 32 and  $76\ \mu\text{m}$  showed very similar dynamics.

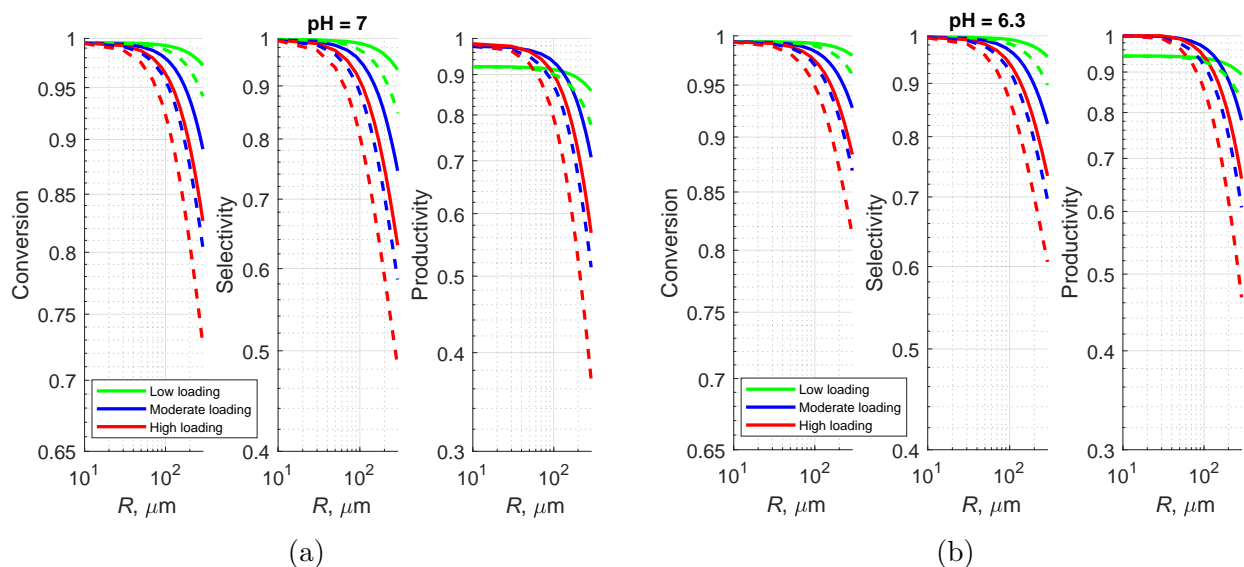


Fig. 6. Batch cephalaxin synthesis process attributes, nucleophile conversion, selectivity, and productivity as a function of carrier size, calculated based on Eqn. (14) and normalized with respect to the free enzyme attributes at the similar condition. Synthesis simulations were performed using  $0.1\ \text{M}$  initial concentration of both substrates, total enzyme concentration of  $5\ \mu\text{M}$ , and at a controlled bulk pH of 7 (a), and 6.3 (b). Solid lines correspond to the carrier with higher effective diffusivities (agarose-like) and dashed lines to Immobead-like carriers. The synthesis process at  $\text{pH} = 6.3$  shows less sensitivity to immobilization and diffusion limitations due to its inherently longer reaction timescale.

Comparing the results for the two APIs in Figure 4, we expect higher sensitivity to diffusion limitations from the ampicillin system, which has a shorter reaction timescale (this

is largely due to higher affinity of PGA for 7-ADCA which improves the SH ratio but results in a slower process [28]). Furthermore, we expect this difference to be stronger at lower enzyme loadings, since at high loadings the reaction becomes significantly faster than diffusion for both systems, making mass transport the rate-determining step. Taking the selectivity as an example attribute, Figure 7 compares the decrease in selectivity due to immobilization for the two APIs. The ampicillin system indeed shows higher sensitivity and selectivity drops faster with increasing carrier size. In line with the previous analysis of Figure 4, this difference in behavior starts to vanish in high enzyme loadings. A similar behavior was also observed for the other process attributes. Note that at high enzyme loadings the deviations from free enzyme attributes for both systems become very close, although the absolute values of the attributes are quite different.

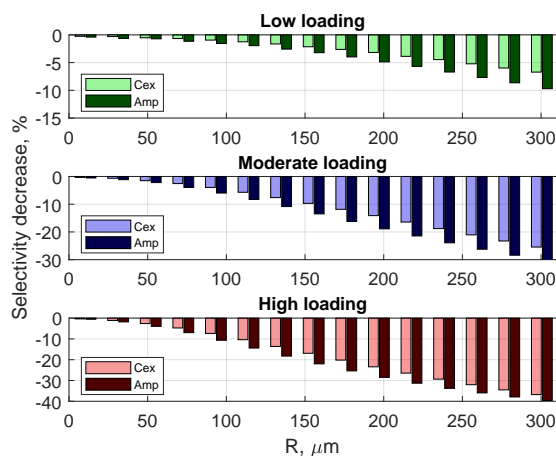


Fig. 7. Decrease in the batch selectivity due to enzyme immobilization on agarose-like carriers with different radii for two systems, ampicillin and cephalixin synthesis (with free enzyme batch selectivity as the reference for each API). Both cases correspond to simulation of a system with 0.1 M initial substrates, and 5  $\mu\text{M}$  total enzyme concentration, and a controlled bulk pH of 7. Ampicillin shows more sensitivity to diffusion limitations due to enzyme immobilization, the difference between the two APIs shrinks at higher enzyme loadings.

Recall that the product is an intermediate in the RN (Figure 1). It should be expected then that the maximum attainable attributes would be those of the soluble enzyme, as shown in Figure 6. The thought process behind this is that the presence of diffusion

resistance leads to API accumulation and hydrolysis before it diffusing out of the biocatalyst hence decreasing the selectivity, conversion and productivity; also, diffusion resistance results in lower concentrations of nucleophile inside the catalyst leading to lower selectivity [28]. However, for a more complete picture, one needs to consider another factor that can significantly affect the enzyme behavior and the reaction rate, is local pH. In the RN of Figure 1, a base (PGME) is consumed to produce an acid (PG). This leads to lower values of pH and potentially a strong pH gradient in systems with large carrier sizes, where the acidic product is at a higher concentration inside the bead (*e.g.*, the internal distribution profile shown in Figure 5b). Deviation of the local pH from that of bulk (which in a batch process is typically controlled at a fixed value by base addition) further alters the enzyme kinetics from its free form at the controlled pH. This secondary effect may lead to further changes in the dynamics (in addition to mass transport) depending on the specific system and process conditions [35]. An example of this is reported by Schroen *et al.* [11], in which using phenylglycine amide as the acyl donor resulted in elevated pHs inside the biocatalyst and faster system dynamics. Examples of experimentally measured pH gradients inside a biocatalyst are reported by Spiess *et al.* [43] for Penicillin G hydrolysis, and Spiess and Kasche [35] for cephalixin synthesis reaction using phenylglycine amide by method of fluorescence microscopy. A pH gradient also has implications with respect to crystallization which will be further discussed in the following sections.

### 3.3 Secondary immobilization variables

In addition to enzyme loading, carrier type, and carrier size, there are two other factors that cannot be controlled as precisely, but may impact the process: (1) enzyme distribution in the biocatalyst, and (2) variance in the carrier size. Here we use the model to investigate whether uncontrolled variations in these parameters can lead to significant deviations from the target operating point in the process and need to be considered for a robust process simulation.

**Enzyme distribution** Considering the large abundance of immobilization sites on porous supports (*e.g.*,  $30 \frac{\mu\text{mol}}{\text{g wet carrier}}$  for ReliZyme [44]), and that during immobilization enzyme diffuses inward from the carrier surface, one may expect higher enzyme concentration in outer regions of the carrier. This has been experimentally confirmed by van Roon *et al.* [45] who used antibody labeling in combination with light microscopy to measure enzyme distribution inside the commercial Assemblase<sup>®</sup> beads. They concluded that as carrier size increased the profile of enzyme distribution showed a steeper decrease from the surface to the carrier center [45].

To study the effect of a nonuniform enzyme distribution, we can still use the information in Figure 6. As was discussed, for both APIs, as the carrier becomes smaller than about 60  $\mu\text{m}$  diffusion limitations become small and all three primary attributes become closely matched to those of the free enzyme. It is reasonable then to assume the same would apply to the case of nonuniform enzyme distribution, meaning that for small beads no significant change in process behavior occurs by varying the enzyme distribution profile, and a simple uniform profile should be sufficient for modeling purposes. Valencia *et al.* [24] assumed a constant enzyme distribution to develop a simplified reaction-diffusion model for cephalixin synthesis using immobilized PGA on 32- and 76- $\mu\text{m}$  radius agarose carriers and experimentally confirmed that their model was robust in predicting concentration profiles. For larger beads diffusion plays a major role, so one might expect a significant change in the process due to nonuniform enzyme distribution. A key point here is that a relatively large carrier with a nonuniform enzyme distribution peaking at its surface can be estimated as a smaller particle with higher enzyme loading (equivalent to that of the high concentration region in original particle). Looking back at Figure 6, predicting the outcome of a nonuniform distribution is not obvious because it is affected by two counteracting factors. Accumulation of the enzyme in outer regions means it is at a higher concentration (*i.e.*, loading) in those regions. However, the effective size of the carrier (*i.e.*, region that contains most of the enzyme) would be smaller under such conditions. The former intensifies the diffusion limitations, unlike

the latter. This interplay gets more complicated considering the impact of the potential pH gradient on enzyme activity. Therefore, even for a carrier with a relatively large radius deciding whether a model needs to take the nonuniform enzyme distribution into account is not obvious. Depending on the specific system and parameters such as carrier size, diffusivities, bulk pH, etc. one might be able to obtain good model predictions while assuming a constant enzyme distribution throughout the biocatalyst. In general, for simulations one can use a function  $e(r)$  to describe the local enzyme concentration in the carrier in Eqn. (2). For consistency, any function  $e(r)$  should be subject to  $\int_0^R e(r)4\pi r^2 dr = N_{enzyme}$  (*i.e.*, total enzyme moles loaded to a bead).

For instance, Figure 8 compares three example enzyme distribution profiles for a cephalixin synthesis simulation using agarose-like carriers. The three enzyme distributions correspond to constant enzyme concentration throughout the carrier or when the majority of the immobilized enzyme is at  $\sim 50$  (Profile 1) and 25 % (Profile 2) of the bead radius. As can be seen, the cephalixin concentration profiles show some dependency on the distribution of the enzyme in the carrier with a large radius. When enzyme is accumulated in close-to-surface regions (Profiles 1 and 2), the system shows a better performance (compared to uniform distribution) in terms of process attributes and achieves a higher conversion. This can be explained by comparing the timescales of reaction and diffusion. Compared to the uniform case, Profile 2 has a higher local enzyme concentration in the active region of the carrier (at its maximum point, approximately 3 times that of the uniform case). On the other hand, the effective size of the carrier is  $\sim 1/3$  of the uniform loading case. Considering that the reaction timescale is inversely proportional to local enzyme concentration, but the diffusion timescale proportional to the square of the carrier size, the positive impact of reducing the effective size on process attributes prevails over the negative impact of higher local enzyme concentration, resulting in mitigation of mass transport limitations and an overall improved process. This is similar to results reported in Ref. [29]. As mentioned, the exact impact of the enzyme distribution can vary depending on specific system under study and parameters

such as overall enzyme loading, carrier size, API system, bulk pH, etc.

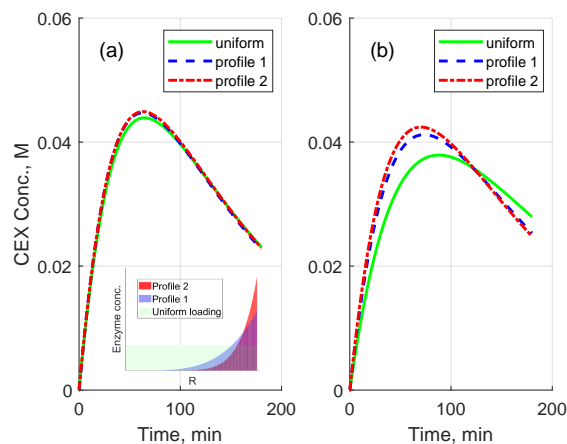


Fig. 8. Effect of different enzyme distribution profiles on API concentration dynamics for a cephalaxin synthesis simulation using immobilized PGA on agarose-like carriers with radius  $100\ \mu\text{m}$  (a), and  $300\ \mu\text{m}$  (b), and with “high” enzyme loading. Total enzyme, and initial acyl donor and nucleophile concentrations are set to  $5\ \mu\text{M}$ , and  $0.1\ \text{M}$  respectively; bulk pH is fixed at 7. Concentration curves from top to bottom at the maximum point correspond to Profile 2, Profile 1, and uniform enzyme distribution.

**Variance in bead size** Commercial porous supports are available in different size ranges, with a size distribution depending on the source and the manufacturing method. Here, we investigate whether different size distributions can lead to significant changes in the simulation results. Following the same logic as the previous section, there is no need to consider the size distribution of carriers in small sizes, as the system dynamics are dominated by the enzymatic kinetics. On the other hand, in samples with a large mean radius, two scenarios occur. For smaller beads in the distribution, diffusion remains unimportant. However, larger beads experience strong diffusion limitations. To approach such systems, one needs to choose one or a series of representative radii to perform the simulations. Note that due to the complex interplay between the reaction kinetics and mass transport (interacting through several parameters such as local pH and enzyme distribution), one single mean size may not be sufficient to represent the behavior of the whole bead sample. In this case, the critical question becomes what is the best method of calculating the mean radius, and whether more than one representative carrier radius needs to be considered for robust

modeling. Also, when multiple representative carrier radii are to be considered in the model, a new challenge arises, that is how should enzyme loading be calculated for individual beads. Further discussion is presented in the Supporting Information (page 4).

Figure 9 shows the results of simulations for cephalexin synthesis using three carrier samples with different sizes and distributions. The simulated API concentration profiles using a single or more representative sizes are compared with the “actual” profile calculated by dividing the carrier size distribution to 9 bins. For Sample 1 with almost all particles smaller than 100  $\mu\text{m}$  radius, a single mean radius is sufficient to accurately mimic the “actual” concentration profile. This was expected since in this size range mass transport-related parameter of radius is almost irrelevant. For Sample 2 with larger beads, simulations based on a single mean size are still able to provide a very good estimation. Sample 3 has the widest distribution with number and volume-based mean radii of 390 and 550  $\mu\text{m}$ . For this sample, a number-based mean radius is not a good candidate for single-size based simulations. A volume-based average radius, however, still provides a good representation. Results of simulations considering multiple bin sizes confirmed that using three bin sizes to represent the total size distribution of carriers results in prediction of concentration profiles almost identical to the “actual” profile, and so is completely sufficient for robust modeling of samples with large and widely distributed particle sizes such as Sample 3. Although, except in extreme cases, size of carrier particles can be safely represented by a volume-based average, it is important to note that smaller beads in sample experience a significantly different concentration profile, and so pH profile, from the larger ones. Solubility of the APIs in these systems is a strong function of pH, and so this has implications with respect to generation of supersaturation inside the biocatalyst in a reactive crystallization process. This will be further discussed in Section 3.4.

As a final note, timescale analysis of Figure 4, and the results presented in Figure 6, obtained by numerical simulation, confirmed that the impact of diffusion on the process depends on the reaction timescale which depends on pH, and the API-specific enzymatic

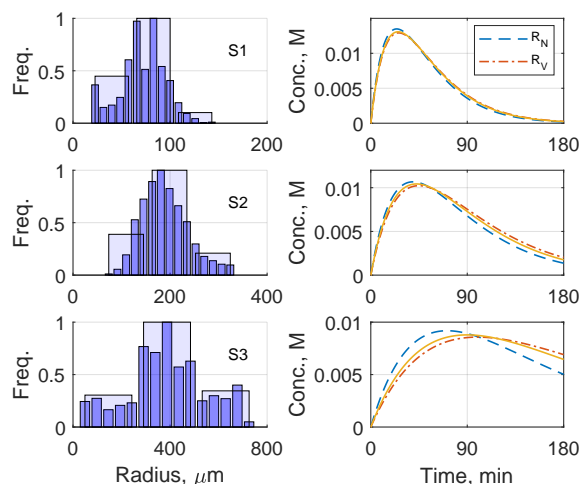


Fig. 9. Comparison of cephalixin concentration profiles for carrier beads with different size distributions for a simulation using  $c_{s0}$  and  $c_{n0} = 0.05$  M and a total enzyme concentration of  $5 \mu\text{M}$  at  $\text{pH} = 8$ . Sample 1 corresponds to commercially available ReliZyme (S), sample 2 to Immobead (COV2), and sample 3 is an artificially constructed sample. Solid curves are “actual” profiles resulting from simulations based on dividing the bead distribution into 9 bins;  $R_N$  and  $R_V$  are results of using one representative average size, number or volume-based. In all cases, considering three bins for representing the carrier size distribution results in a concentration profile almost identical to the “actual” profile.

kinetics. However, considering the complexities in the rate equation (*e.g.*, inhibitory effects of nucleophile), timescale of enzymatic reaction described by Eqn. (1) also depends on substrate concentrations (unlike for example, a simple reaction network of  $A \rightarrow B$ ). Therefore, observed loss in enzyme activity or process attributes due to immobilizing the enzyme also depends on specific substrate concentrations used [27]. Figure 10 illustrates the simulated drop in initial SH ratio  $\left(\frac{c_p}{c_b}\right)_{t=\epsilon}$  for a cephalixin synthesis simulation using different carriers for a range of pHs and substrate concentrations. As expected, the carrier with highest diffusivity and smaller radius shows the least drop in performance. Decreasing the pH also leads to less sensitivity to mass transport limitations since the overall reaction is slower at lower pHs. Similarly, using larger initial concentrations results in longer reaction timescale, leading to the same behavior. Comparable losses in SH ratio were reported by Janssen *et al.* [28], where performing cephalixin synthesis using 0.15 and 0.1 M substrate concentrations and PGA immobilized on Eupergit carriers resulted in selectivity loss as high as 75% [28]. Similar

figure for the ampicillin synthesis is presented in the Supporting Information (Figure S4).

Reaction kinetic parameters in Eqn. (1) are typically measured using initial-rate experiments. The aforementioned point implies that performing such experiments for immobilized enzyme, one cannot generalize the drop in the enzyme activity and SH ratio measured at a specific concentration to other reaction conditions. This highlights another benefit of using a reaction-diffusion model for studying systems with immobilized enzyme. Taking this approach, one can approximate the loss in activity and SH ratio upon immobilization for different substrate concentrations without performing initial-rate experiments.

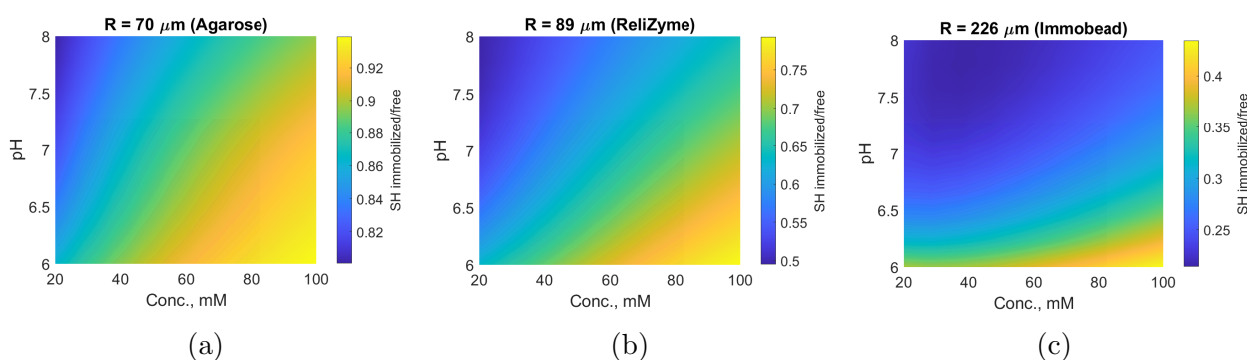


Fig. 10. Simulations of synthesis-to-hydrolysis ratios in initial-rate experiments at different initial substrate concentrations and pHs for different enzyme carriers. An initial-rate experiment was simulated by setting the total enzyme concentration at  $1 \mu\text{M}$  and allowing the synthesis to proceed for 5 min. For all simulations a “high” enzyme loading on carrier with a nonuniform enzyme distribution (Profile 1 in Figure 8) was used. Each graph shows the initial SH ratio using the specific carrier, normalized with respect to the free enzyme ratio under the same condition.

### 3.4 Crystallization

At conditions typically used in a synthesis experiment, products are formed at concentrations above their solubility limit leading to nucleation and growth of crystals from the solution. Crystallization is beneficial to the process as it protects the product from hydrolysis. Crystallization affects dynamics of species concentrations by consuming the supersaturated species (*e.g.*, cephalixin) which in turn alters rate of the hydrolysis in the RN of Figure 1. Including crystallization in the process model enables both the study of differ-

ent enzymatic reactive crystallization processes using specific carriers and rational decisions regarding process design. To illustrate, consider designing a batch process for either production of cephalexin monohydrate or ampicillin trihydrate crystals using the commercial ReliZyme as carrier (Sample 1 in Figure 9). PGA activity increases with pH, but the solubility of both APIs also sharply increases at pHs above 7, which hinders crystallization. Figure 11 compares four different scenarios for operating this process starting with initial concentrations of 0.3 M and 0.2 M for the activated acyl donor and the nucleophile reactant, respectively. Case (a) corresponds to simulation of a process with constant pH of 7, while case (b) corresponds to the same starting state but without bulk pH control. Cases (c) and (d) have the same pH control strategies as Cases (a) and (b), respectively but for a system initially seeded with 1 *wt%* API crystals (calculated based on equivalent crystal mass of the initial nucleophile concentration). In each case, the simulation is stopped when byproduct, PG, concentration reaches 0.05 M. As mentioned, PG also has a limited solubility in water and exceeding this concentration will cause PG crystals to form and contaminate the product [21]. It is possible to include the PG crystallization in the model by adding additional elements to the system state vector  $\vec{u}$ . However, since the main goal is to avoid PG crystal formation (and not to measure its accumulation), one can track its concentration and design the process in a way that it remains below the solubility or, if slightly above, only for a short period of time, to avoid nucleation in the metastable zone, and subsequent growth.

Analyzing Figure 11, mass of cephalexin crystals produced in the best case is about half that of the ampicillin. This is mainly due to significantly higher solubility of cephalexin leading to a significant portion of the synthesized API remaining in the solution phase. Also the ampicillin process proceeds faster which was expected from its generally shorter reaction timescale (Figure 4), and faster crystal growth rate. Based on the simulations, for both systems the best strategy for operating a batch process is not to control the pH and instead let it drop over the course of the reaction [36]. While a drop in pH decreases the enzyme activity, its impact on solubility is larger, leading to higher supersaturation and therefore,

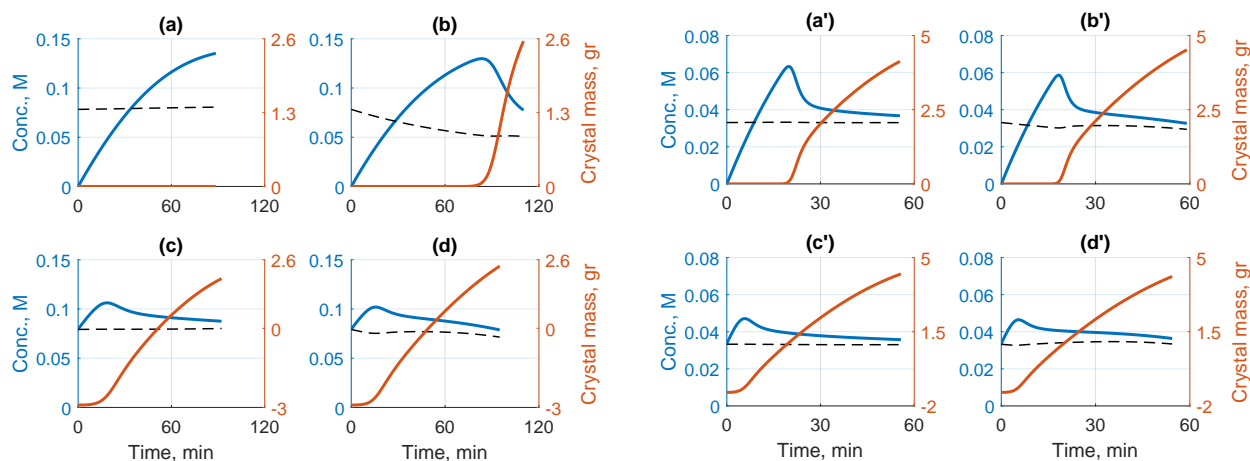


Fig. 11. Comparison of different strategies for production of cephalexin (left) and ampicillin (right) crystals in a batch reactive crystallization process using immobilized enzyme. Simulations were performed for  $c_{s0} = 0.3$  M,  $c_{n0} = 0.2$  M,  $\text{pH}_0 = 7$ , and total enzyme concentration of  $5 \mu\text{M}$ , immobilized on ReliZyme (S) carriers with “high” loading level. Cases (a) and (b) correspond to unseeded batches with controlled and uncontrolled bulk pH, respectively. Cases (c) and (d) correspond to similar systems seeded with 1 wt% API crystal seeds with an average seed crystal size of  $5 \mu\text{m}$ . Left axis shows the API concentration, and the right axis shows the net mass of crystals produced in a reactor with 100 mL volume. Dashed lines show the thermodynamic solubility which slightly changes during the process due to either base addition (Cases a and c) or decrease in pH (Cases b and d). For seeded cases, the initial crystal mass is negative to take into account the necessary amount of API needed to saturate and seed the initial solution. Each simulation is stopped when byproduct PG concentration reached 0.05 M. Best case for cephalexin synthesis results in 74% nucleophile conversion compared to 67% when no crystallization is considered in the simulation. These values are 72% versus 55% for the ampicillin synthesis.

rate of crystallization. Moreover, the enzyme SH ratio slightly increases at lower pH which is beneficial to the process. Also note that the difference due to different pH control strategies is smaller for ampicillin system; this was expected from Figure S1 and that ampicillin solubility is less sensitive to pH compared to cephalexin.

Comparing cases with or without initial seeding, generally seeding is beneficial and results in higher process yield and productivity. For the cephalexin system with fixed pH (Cases a and c), seeding is critical because the rate of primary nucleation is insufficient to lead to significant crystal formation before the PG concentration reaches saturation, stopping the simulation. For ampicillin both cases result in similar final crystal mass, the difference is par-

tially due to the fact that reported primary nucleation parameters for ampicillin trihydrate are larger than cephalixin monohydrate crystals [16, 15]. Therefore, ampicillin generates more nuclei in a shorter time than cephalixin; the nuclei can grow and contribute to secondary nucleation. In an unseeded batch process, primary nucleation is critical in initiation of crystallization after which secondary nucleation becomes the dominant nuclei generating mechanism [46]. Nevertheless, from a practical standpoint, seeding batch processes is usually desirable since it helps to control the final CSD and crystal shape, and provides better consistency in product quality [46]. Furthermore, being an intrinsically stochastic process, it is challenging to introduce the uncertainties associated with primary nucleation to the model [16]. This can result in potentially significant deviation from simulations and variance between different batches in practice. Also, note that in both systems, cases with no seeding experience much higher levels of supersaturation (difference between the solubility line and API concentration). High supersaturation can negatively affect the shape of crystals as it is reported that higher supersaturation leads to higher aspect-ratio crystals in these systems, introducing challenges to downstream filtration steps [39, 47]. Control of supersaturation is another motivation for seeding batch reactive crystallization. In a continuous process, the crystal population present in the vessel at steady-state serves as the principal source of nuclei through secondary nucleation to keep the supersaturation at a desired level; here, the impact of primary nucleation is most important for the initial startup phase.

Information in Figure 11 serves as an example of how the presented method can be applied to make decisions about design of a reactive crystallizer for synthesis of APIs. While in this example total crystal mass produced was taken as the single most important process attribute and the benchmark criterion, in a broader scope of the process there are other factors that are as important (if not more) in the final process design. As mentioned, the biocatalyst activity typically increases with pH value, leading to higher reaction rates and shorter reaction times. In contrast, crystallization is enhanced at lower pH values, encouraged by the lower solubility of the API. This trade-off manifests itself in the process

volumetric productivity which is a more representative attribute in evaluating a process than crystal yield. As an example, Figure S5 in the Supporting Information compares the batch process volumetric productivity of the crystals under different control pH values for both APIs. While higher pH values lead to significantly shorter process times, impact of pH on drug solubility causes the volumetric productivity to drop at pH values above a certain API-dependent value. Another important factor in determining the truly optimum process is the process yield. The overall yield in terms of the costlier reactant, the  $\beta$ -lactam core, can have a significant impact on the production cost. Considering that both APIs of interest are generic drugs, the cost of 7-ADCA or 6-APA can have a major impact on the techno-economic analysis of the process, potentially surpassing that of the productivity. Furthermore, when finding the optimum design for the reactive crystallization, other process units besides the reaction vessel must be considered. For example, crystallization is typically followed by filtration and washing steps in the pharmaceutical industry to ensure purity of the crystal product. Performing the simulations of a reactive crystallizer presented in Figure 11, the maximum permissible phenylglycine (reaction byproduct and a potential impurity) concentration was set to 50 mM, and that was used as the criterion to halt the simulations. However, depending on the robustness of the downstream crystal washing steps, the allowed limit for phenylglycine concentration may be set higher. Clearly, this can alter the outcome and our interpretation of the simulations and change the optimum design point based on process modeling. Taking such considerations into account is necessary for designing an industrially-relevant process and needs to accompany the type of analysis presented in this work to approach this multi-objective problem.

### **Local pH and supersaturation**

Independent of pH control strategy, there will be concentration gradients, and consequently pH gradients, developed inside the biocatalyst bead. Using a buffer in the solution can help mitigate this effect, but that is not always practical in large-scale processes. The exact pH profile would vary case to case based on factors such as carrier type, radius, en-

zyme distribution inside the carrier, concentrations, etc. As an example, Figure 12 shows the developed pH profile at the last time point in the cephalixin reactive crystallization process simulated above, when the system is not seeded and bulk pH is controlled at its set value by addition of NaOH (Case (a)).

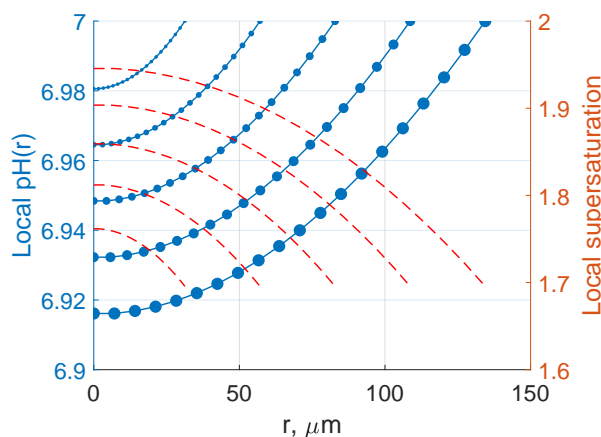


Fig. 12. Local pH profile inside the beads with different radii (30, 60, 80, 110, 135  $\mu\text{m}$ ) in a ReliZyme carrier sample at the last time point for the cephalixin synthesis simulation of Figure 11, Case (a), bulk pH is controlled at 7. Dashed lines show the local supersaturation level calculated based on the API solubility at the local pH. Spatial node markers for larger beads in the sample are shown larger.

As it can be seen in Figure 12, due to consumption of the basic reactant, PGME, local pH is lower inside the carrier, where reaction occurs, than that of the bulk. The gradient becomes steeper as the size of the bead increases due to stronger mass transport limitations. As mentioned, solubility decreases at lower pH values which leads to a higher supersaturation inside the biocatalyst compared to the bulk. In an unseeded batch process such as Cases (a) and (b) in Figure 11, where the system goes through periods of relatively high supersaturation (or an equivalent condition in a continuous process startup) this results in an even higher local supersaturation within the carrier. This is not desired since it can lead to nucleation and growth of crystals inside the pores of carrier which can, at least partially, deactivate the biocatalyst. Analyzing Figure 12, larger beads in a sample are more susceptible to intra-bead crystallization compared to the smaller ones (that follow the bulk pH more closely). Again, it is desired to keep the supersaturation levels low by seeding the system. Figure 13 shows

the same analysis of local pH and supersaturation inside the carrier for the seeded scenario in Figure 11 (Case (c)). In any case, a raw estimation for the probability of nucleation inside the biocatalyst can be made using the rate of primary nucleation at a certain supersaturation; this is related to the concept of induction time that is the time required for a significant and detectable nucleation to occur at a fixed supersaturation ( $t_{ind} \propto 1/B_1$ ). For example, according to McDonald *et al.* [16], a supersaturated solution of cephalexin at  $S = 1.98$  can take about 1 – 3 hr to produce significant nucleation. At  $S = 1.6$  this can take as long as 10 hr. Therefore, even at a significant supersaturation of  $S = 1.5$ , continuous production of cephalexin would not be expected to result in substantial primary nucleation within the bead.

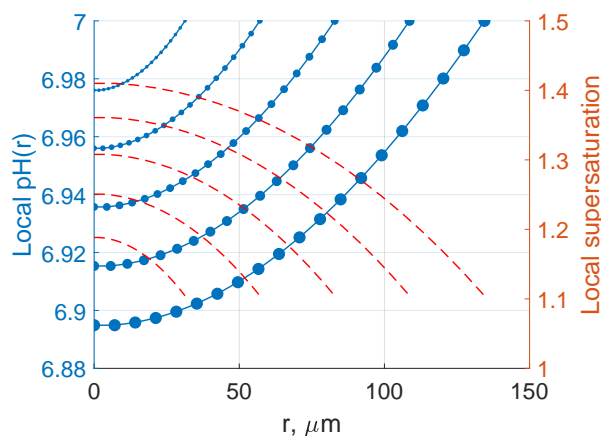


Fig. 13. Local pH profile inside the beads with different radii (30, 60, 80, 110, 135  $\mu\text{m}$ ) in a ReliZyme carrier sample at the last time point for the seeded cephalexin synthesis simulation of Figure 11, Case (c). Dashed lines show the local supersaturation level calculated based on the API solubility at the local pH. Spatial node markers for larger beads in the sample are shown larger.

It is worth highlighting that local pH and supersaturation profiles presented in Figures 12 and 13 are just example cases. Local supersaturation in a biocatalyst in a batch process spans a wide range of values depending on not just carrier radius, bulk pH, enzyme distribution profile, and concentrations but also the process time. pH gradient analysis becomes more critical in designing continuous processes where system parameters should be chosen

such that the supersaturation inside the carrier at steady-state is kept as low as possible.

Calculations of local supersaturation are based on the assumption that API solubility is only a function of pH and ionic strength. However, this might not be the case in a confined environment such as pores of a carrier. The concept of pore size dependent solubility is well documented in the geology literature as it is necessary for estimation of the crystallization rate of minerals and salts in rocks [48]. It is generally the case that crystallization in pores requires higher supersaturation due to the restriction of crystal growth by the pore walls affecting the interfacial energy, known as the Gibbs-Thomson effect [48, 49]. For example, Rijniers *et al.* [50] used Nuclear Magnetic Resonance (NMR) spectroscopy to show that the solubility of  $\text{Na}_2\text{CO}_3$  in 10 nm pores at 10 °C can be as much as three times the solubility of the bulk. This effect has also been reported for porous enzyme carriers. Kasche and Galunsky [51] used the penicillin amidase enzyme immobilized on a variety of carriers with different pore sizes to study the reaction of hydrolysis of D-phenylglycine amide to phenylglycine at high concentrations leading to product precipitation. In agreement with the above studies, they showed that carriers with smaller pore sizes (10 – 30 nm) retain most of their activity after multiple experiments, implying less enzyme blockage due to crystallization in the pores. However, for carriers with larger pores, a significant portion of activity is lost over 3 consecutive uses in batch experiments (for comparison, ReliZyme carriers reportedly have a 40 – 60 nm pore diameter [44]). One can postulate that for a carrier with a pore size distribution, larger pores might be blocked by API crystals after some time, however, the enzyme immobilized in smaller pores remains accessible and active. In such cases an initial decrease followed by a leveling in enzyme activity is expected upon using the carrier in multiple experiments. Another possible solution to the high local supersaturation issue is to use the D-phenylglycine amide as the activated acyl donor in Figure 1, which releases an ammonia molecule upon binding to the enzyme. This results in increasing the local pH and consequently API solubility at reaction centers. In this case the bulk pH needs to be controlled at the fixed level by addition of an acid [29].

## 4 Conclusion

A process model for reactive crystallization of  $\beta$ -lactam antibiotics using immobilized enzyme was developed. Three kinetic phenomena were considered: enzymatic reaction, diffusion in a porous biocatalyst bead, and crystallization of supersaturated species. A mathematical model and a numerical simulation procedure were used to explore the interplay among the governing phenomena and the system dynamics. Previously established parameters based on Michaelis–Menten enzyme kinetics, which included effects of pH on reactivity and inhibition, were used. Crystallization was described using a population balance model with kinetic data from the literature. Diffusion in the catalyst support was modeled using a continuum approach by defining effective diffusivities for each species. Key assumptions in the model were: (1) the reaction kinetics for the immobilized enzyme was the same as for the free enzyme (*i.e.*, no significant conformational changes during immobilization and negligible electrostatic and steric effects), and (2) API crystals formed only in the bulk phase. The measured effective diffusivity lumped together the effects of all parameters, such as carrier hydrophobicity, tortuosity, surface charge, etc., to the effective diffusion coefficient and assumed similar interaction with the carrier matrix for all species. Also, no external mass transport resistance was assumed in the boundary layer around the biocatalyst. Moreover, this study assumed a constant temperature of 25 °C at which most of the parameters have been reported. This model can be extended to other temperatures by accounting for the effect of temperature on enzyme kinetics, effective diffusivities, and API solubility.

Comparing the numerical simulation results with timescale analysis showed that insight can be gained into the interplay between the enzymatic reaction and diffusion processes before performing detailed calculations. As expected, both approaches showed that reactions with shorter timescales are more sensitive to mass transport limitations. The timescale of an enzymatic reaction in general was shown to depend on API-specific reaction kinetics, solution pH, and concentration of substrates. This results in different deviations from free enzyme, as

a reference, for processes performed under different conditions, and highlights the necessity of developing detailed mathematical models. The developed reaction-diffusion model also allowed for systematically analyzing the impact of different enzyme immobilization variables, such as enzyme loading and distribution, bead size, and bead size distribution and structure. Coupling a crystallization module to the reaction-diffusion model allowed for describing the system under a wide range of conditions including those where significant supersaturation is generated and leads to crystal nucleation and growth, as in reactive crystallization.

As with every model, the accuracy of the simulations is at the mercy of accurate input parameters. Enzymatic reaction parameters are typically measured using initial-rate experiments for a specific enzyme variant, and can be refined to better represent the time course of the reaction. An alternative approach to decoupling the reaction and diffusion is lumping both steps and use experimental data from immobilized enzyme activity measurements to define a set of kinetic parameters for a specific biocatalyst (such as Ref. [11]). Application of such parameters and the developed kinetic model, however, remains limited to the specific case for which the parameters were determined.

The highest uncertainty in the model is associated with calculating the supersaturation in the crystallization module. As mentioned, API solubility in general is a function of pH, temperature, ionic strength and the concentration of cosolutes. Measuring solubility as a function of pH becomes more challenging at values close to the  $pK_a$ , where changes become more significant. Measuring the impact of cosolutes on solubility is also challenging and requires extensive experimentation to cover the range of potential concentrations. However, this is less important in a continuous process which is designed to operate at a fixed point at steady-state. Nevertheless a general understanding of the impact of cosolutes is necessary even in designing a continuous process.

Overall, immobilizing the enzyme introduces some level of mass-transfer resistance to the system. Longer presence of the product in the reactive environment of the carrier leads to higher rates of hydrolysis. Moreover, limited diffusion of nucleophile to active sites results in

attack of abundant water molecules to acyl-enzyme complex, lowering the SH ratio. To avoid these, it is desirable to use an immobilization carrier with a small radius and a highly porous structure to minimize the mass transfer resistance. However, designing a reactive crystallization process, a carrier candidate cannot be selected without taking the catalyst/product separation and carrier structural integrity related issues into account. The type of analysis presented in this work is helpful in identifying how significant is the impact of using larger or less porous beads on a specific process in order to weigh these considerations.

## Conflict of interest

Authors declare no conflict of interests.

## Acknowledgment

Authors would like to thank the U.S Food and Drug Administration Center for Drug Evaluation and Research for financial support through Grant U01FD006484.

## References

- [1] H. Gelband, M Miller-Petrie, S. Pant, S. Gandra, J. Levinson, D. Barter, A. White and R. Laxminarayan, *Wound Healing Southern Africa*, 2015, **(2)**, 30-34.
- [2] R. B. Hamed, J. R. Gomez-Castellanos, L. Henry, C. Ducho, M. A. McDonough and C. J. Schofield, *Natural Product Reports*, 2013 **30(1)**, 21-107.
- [3] R. C. Giordano, M. P. Ribeiro and R. L. Giordano, *Biotechnology Advances*, 2006, **24(1)**, 27-41.
- [4] M. I. Youshko, G. G. Chilov, T. A. Shcherbakova and V. K. Svedas, *Biochimica et Biophysica Acta (BBA)-Proteins and Proteomics*, 2002, **1599(1-2)**, 134-140.
- [5] M. Y. Gololobov, E. V. Kozlova, I. L. Borisov, U. Schellenberger, V. Schellenberger and H. D. Jakubke, *Biotechnology and Bioengineering*, 1992, **40(3)**, 432-436.
- [6] E. M. Gabor and D. B. Janssen, *Protein Engineering Design and Selection*, 2004, **17(7)**, 571-579.
- [7] M. A. McDonald, A. S. Bommarius and R. W. Rousseau, *Chemical Engineering Science*, 2017, **165**, 81-88.

- [8] M. I. Youshko and V. K. Svedas, *Biochemistry (Moscow)*, 2000, **65(12)**, 1367-1375.
- [9] D. Hulsewede, L. E. Meyer and J. von Langermann, *Chemistry – A European Journal*, 2019, **25(19)**, 4871-4884.
- [10] P. Valencia, L. Wilson, C. Aguirre and A. Illanes, *Enzyme and Microbial Technology*, 2010, **47(6)**, 268-276.
- [11] C. G. P. H. Schroen, C. B. Fretz, V. H. DeBruin, W. Berendsen, H. M. Moody, E. C. Roos, J. L. VanRoon, P. J. Kroon, M. Strubel, A. E. M. Janssen and J. Tramper, *Biotechnology and Bioengineering*, 2002, **80(3)**, 331-340.
- [12] L. R. Goncalves, R. Sousa, R. Fernandez-Lafuente, J. M. Guisan, R. L. Giordano and R. C. Giordano, *Biotechnology and Bioengineering*, 2002, **80(6)**, 622-631.
- [13] M. Ottens, B. Lebreton, M. Zomerdijk, M. P. W. M. Rijkers, O. S. L. Bruinsma and L. A. M. van der Wielen, *Industrial & Engineering Chemistry Research*, 2001, **40(22)**, 4821-4827.
- [14] M. Santana, M. P. Ribeiro, G. A. Leite, R. L. Giordano, R. C. Giordano and S. Mattedi, *AIChE Journal*, 2009, **56(6)**, 1578-1583.
- [15] L. G. Encarnacion-Gomez, A. S. Bommarius and R. W. Rousseau, *Industrial & Engineering Chemistry Research*, 2016, **55(7)**, 2153-2162.
- [16] M. A. McDonald, G. D. Marshall, A. S. Bommarius, M. A. Grover and R. W. Rousseau, *Crystal Growth & Design*, 2019, **19(9)**, 5065-5074.
- [17] C. R. Malwade and H. Qu, *Current Pharmaceutical Design*, 2018, **24(21)**, 2456-2472.
- [18] Y. Fan, Y. Li and Q. Liu, *Biotechnology and Applied Biochemistry*, 2020.
- [19] A. B. Cuthbertson, A. D. Rodman, S. Diab and D. I. Gerogiorgis, *Processes*, 2019, **7(6)**, 318.
- [20] A. Dafnomilis, S. Diab, A. D. Rodman, A. G. Boudouvis and D. I. Gerogiorgis, *Industrial and Engineering Chemistry Research*, 2019, **58(40)**, 18756-18771.
- [21] M. A. McDonald, A. S. Bommarius, R. W. Rousseau and M. A. Grover, *Computers & Chemical Engineering*, 2019, **123**, 331-343.
- [22] C. R. Thomas and P. Dunnill, *Biotechnology and Bioengineering*, 1979, **21(12)**, 2279-2302.
- [23] A. I. Kallenberg, F. van Rantwijk and R. A. Sheldon, *Advanced Synthesis & Catalysis*, 2005, **347**, 905-926.
- [24] P. Valencia, S. Flores, L. Wilson and A. Illanes, *New Biotechnology*, 2012, **29(2)**, 218-226.

- [25] P. Grunwald, *Biochemical Education*, 1989, **17(2)**, 99-102.
- [26] L. R. Goncalves, R. Fernandez-Lafuente, J. M. Guisan, R. L. Giordano and R. C. Giordano, *Biotechnology and Applied Biochemistry*, 2003, **38(1)**, 77-85.
- [27] M. L. Shuler, F. Kargi, M. DeLisa, *Bioprocess Engineering: Basic Concepts, Ch. Enzymes*, Pearson, 3rd Ed., 2017.
- [28] M. H. Janssen, L. M. van Langen, S. R. Pereira, F. V. Rantwijk and R. A. Sheldon, *Biotechnology and Bioengineering*, 2001, **78(4)**, 425-432.
- [29] J. L. van Roon, M. M. H. D. Arntz, A. I. Kallenberg, M. A. Paasman, J. Tramper, C. G. P. H. Schroen and H. H. Beftink, *Applied Microbiology and Biotechnology*, 2006, **72(2)**, 263-278.
- [30] C. Karakaya, P. J. Weddle, J. M. Blasi, D. R. Diercks and R. J. Kee, *Chemical Engineering Science*, 2016, **145**, 299-307.
- [31] M. A. Sadeghi, M. Aganou, M. Kok, M. Aghighi, G. Merle, J. Barralet and J. Gostick, *Journal of The Electrochemical Society*, 2019, **166(10)**, A2121-A2130.
- [32] H. S. Fogler, *Elements of Chemical Reaction Engineering*, Pearson Education, 4th Ed., 2006.
- [33] F. Pohlmann and A. Jess, *Catalysis Today*, 2016, **275**, 172-182.
- [34] P. Dechadilok and W. M. Deen, *Industrial and Engineering Chemistry Research*, 2006, **45(21)**, 6953-6959.
- [35] A. C. Spiess and V. Kasche, *Biotechnology Progress*, 2001, **17(2)**, 294-303.
- [36] M. B. Diender, A. J. J. Straathof, T. Van der Does, M. Zomerdijk and J. J. Heijnen, *Enzyme and Microbial Technology*, 2000, **27(8)**, 576-582.
- [37] E. I. Volcke, S. Van Hulle, T. Deksissa, U. Zaher and P. A. Vanrolleghem, *BIOMATH*, Ghent University, Ghent, 2005.
- [38] J. M. Prausnitz, R. N. Lichtenthaler and E. G. De Azevedo, *Molecular Thermodynamics of Fluid-phase Equilibria*, Prentice-Hall, 3rd Ed., 1998.
- [39] M. Li, Z. Shang and B. Hou, *Transactions of Tianjin University*, 2019, **25(4)**, 348-356.
- [40] A. Chianese, *Industrial Crystallization Process Monitoring and Control*, 2012.
- [41] K. B. Bischoff, *AIChE Journal*, 1965, **11(2)**, 351-355.
- [42] P. Valencia and F. Ibanez, *Catalysts*, 2019, **9(11)**, 930.
- [43] A. Spiess, R. C. Schlothauer, J. Hinrichs, B. Scheidat and V. Kasche, *Biotechnology and Bioengineering*, 1999, **62(3)**, 267-277.

- [44] Product Technical Data Sheet, ReliZyme EP403, Resindion, Italy.
- [45] J. L. van Roon, E. Groenendijk, H. Kieft, C. G. P. H. Schroën, J. Tramper and H. H. Beftink, *Biotechnology and Bioengineering*, 2005, **89(6)**, 660-669.
- [46] A. Lewis, M. Seckler, H. Kramer and G Van Rosmalen, *Industrial Crystallization: Fundamentals and Applications*, Cambridge University Press, Cambridge, 2015.
- [47] G. Perini, F. Salvatori, D. R. Ochsenein, M. Mazzotti and T. Vetter, *Separation and Purification Technology*, 2019, **211**, 768-781.
- [48] R. J. Flatt, *Journal of Crystal Growth*, 2002, **242(3-4)**, 435-454.
- [49] G. W. Scherer, *Cement and Concrete research*, 1999, **29(8)**, 1347-1358.
- [50] L. A. Rijniers, H. P. Huinink, L. Pel and K. Kopinga, *Physical Review Letters*, 2005, **94(7)**, 075503.
- [51] V. Kasche and B. Galunsky, *Biotechnology and Bioengineering*, 1995, **45(3)**, 261-267.

## Table of content entry

A mathematical model for production of  $\beta$ -lactam antibiotics via enzymatic reactive crystallization is developed, its application for catalyst and process design is discussed.

